

Laser Interferometric Sensor for seismic waves velocity measurement

Fausto Acernese^{a,c}, Rosario De Rosa^{b,c}, Fabio Garufi^{b,c}, Rocco Romano^{a,c} and Fabrizio Barone^{a,c}

^a Dipartimento di Scienze Farmaceutiche, Università degli Studi di Salerno, Via Ponte Don Melillo, I-84084 Fisciano (SA), Italia

^b Dipartimento di Scienze Fisiche, Università degli Studi di Napoli Federico II, Complesso Universitario di Monte S. Angelo, Via Cintia, I-80126 Napoli, Italia

^c INFN Sezione di Napoli, Complesso Universitario di Monte S. Angelo Via Cintia, I-84084 Napoli, Italia

ABSTRACT

Laser interferometry is one of the most sensitive methods for small displacement measurement for scientific and industrial applications, whose wide diffusion in very different fields is due not only to the high sensitivity and reliability of laser interferometric techniques, but also to the availability of not expensive optical components and high quality low-cost laser sources. Interferometric techniques have been already successfully applied also to the design and implementation of very sensitive sensors for geophysical applications.¹ In this paper we describe the architecture and the expected theoretical performances of a laser interferometric velocimeter for seismic waves measurement. We analyze and discuss the experimental performances of the interferometric system, comparing the experimental results with the theoretical predictions and with the performances of a state-of-the-art commercial accelerometer. The results obtained are very encouraging, so that we are upgrading the system in order to measure the local acceleration of the mirrors and beam splitter of the velocimeter using an ad hoc designed monolithic accelerometers for low frequency direct measurement of the seismic noise.

Keywords: Velocimeter, Seismic Sensor, Laser Interferometry

1. INTRODUCTION

The most common differential length measurement is a measurement of the length fractional change of a given baseline, referred in geophysics as local strain. The magnitudes of the strains encountered in practice are spread over a wide range: Earth-tide strain may be as large as 10^{-7} while strains produced by teleseismic earthquakes rarely exceed 10^{-9} . The strain noise at quiet sites has been measured by Berger and Levine,² who used data from very different instruments located about 2000 *km* apart in very different geological conditions. Nevertheless, their results are in good agreement over the frequency range extending from approximately 1 *cycle · month*⁻¹ to several *cycles · sec*⁻¹. Therefore, it seems reasonable to assume that their results represent a reasonable estimate of the earth noise.

There are many kinds of instruments adequate for the observations of seismic signals. The periods of these signals are of the order of seconds or minutes and these periods are sufficiently short (relatively speaking) so that considerations on the instrument long-term stability or on its sensitivity to slowly changing environmental parameters (such as environmental temperature) are usually not so relevant for the design success. In particular, a strainmeter is generally considered adequate for a measurement if it is limited by earth noise over its whole operating frequency range. On the other hand, the secular stability and the residual sensitivity to external noise sources like the environmental temperature usually completely dominates the noise budget of instruments designed to observe signals with periods of a few hours or longer. The residual sensitivity to fluctuations of the environmental temperature or of the barometric pressure often sets a lower-bound on the minimum detectable

Send correspondence to Prof. Fabrizio Barone - E-mail: fabrizio.barone@na.infn.it

vibration level which is independent from the intrinsic resolution of the sensor or from the amplification of its read-out system.

Laser interferometry³ is one of the possible techniques to design a sensor for seismic wave measurement. In this paper we describe the architecture of a laser interferometric sensor developed for geophysical applications, to be used as a velocimeter for seismic waves detection, that is an improvement of a system we began to develop some years ago^{4,5}. Particular attention was given to the definition of the theoretical model, necessary also for the choice of optimal system parameters. The performances of the interferometric system are analyzed, both theoretically and experimentally, and then compared to a standard state-of-the-art commercial accelerometer. The results obtained are very encouraging, so that we are upgrading the system in order to measure the local acceleration of the mirrors and beam splitter of the velocimeter using ad hoc designed monolithic accelerometers for low frequency direct measurement of the seismic noise.¹¹

2. MODEL OF INTERFEROMETRIC SEISMIC SENSOR

2.1 Optical Model

The best and most versatile interferometric device is the interferometer developed by Michelson in 1880. The basic scheme is shown in Figure 1. In a Michelson Interferometer, the beam from the laser source is splitted

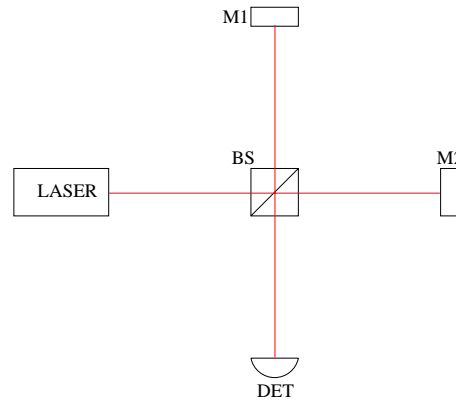


Figure 1. Optical scheme of a Michelson Interferometer

by the Beam Splitter BS into two beams, that are then reflected back to BS by the mirrors M_1 and M_2 . The interference pattern is observed on the detector plane, DET .

Assuming a plane wave beam, then the Michelson Interferometer output, $I(t)$, can be generally expressed as

$$I(t) = I_{min} + \frac{I_{max} - I_{min}}{2} [1 + \cos(\phi(t))] \quad (1)$$

where $\phi(t)$ is the phase difference between the two beams, and I_{max} and I_{min} are the maximum and the minimum output intensities, respectively. In particular, the maximum value of the intensity is reached when the two beams are recombined in phase, while the minimum is instead obtained when they are recombined in opposition of phase. Generally, these quantities are time dependent, but for a Michelson Interferometer with well aligned mirrors and nearly equal arm lengths, negligible laser source amplitude noise and coherence length of the laser source much longer than the arm-lengths, we can consider them constant. Therefore, the only time dependent quantity in Equation 1 is the phase change $\phi(t)$, that can be expressed as

$$\phi(t) = \frac{4\pi n(t)}{\lambda(t)} \left\{ [l_2(t) - l_1(t)] + \sum_{i=1}^2 [l_i(t) + d] \sum_{j=1}^2 \theta_{i,j}^2 \right\} \quad (2)$$

where $\lambda(t)$ is the laser beam wavelength, $n(t)$ is the spatial mean refraction index, $l_i(t)$ is the i^{th} arm-length, d is the distance of the beam-splitter from the output photodiode, and $\theta_{i,j}$ is the j^{th} tilt of the mirror in the i^{th} arm.

All these functions are in principle time dependent. But, since very effective techniques exist for the alignment control of the optics, it is possible to assume the hypothesis of a perfectly aligned system, so that Equation 2 can be written as

$$\phi(t) = \frac{4\pi n(t)}{\lambda(t)} l_{eq}(t) \quad (3)$$

where $l_{eq}(t) = l_2(t) - l_1(t)$ is the longitudinal Michelson Interferometer arm-length difference, that is, of course, a time dependent function. Then, to extract the arm-length change due to the presence of a seismic wave, we choose one arm as reference, mechanically fixing its length and screening it from refraction index changes, which may simulate mechanical length changes. The other arm, that is the measurement arm, is instead allowed to change its length in order to measure the passage and the amplitude of a seismic wave.

In this model we did not take into any account the effects of the mirror mechanical mounts in the measurement band of the interferometer. If we assume that the mechanical mounts are linearly coupled with the interferometer, then the interferometer output can be expressed as the convolution of the input signal and the mechanical mounts impulse response, that is:

$$\Delta l_{eq}(t) = k_2(t) * l_2(t) - k_1(t) * l_1(t) \quad (4)$$

where $k_1(t)$ and $k_2(t)$ are the mechanical mount impulse response relative to mirror 1 and to mirror 2, respectively. In particular, if the mechanical mounts are the same for both the mirrors then $k_1(t) = k_2(t) = k(t)$ and $l_{eq}(t) = k(t) * (l_2(t) - l_1(t))$. Furthermore, taking into account that the resonance frequencies of the optical holders are generally enough high not to produce effects in the measurement band of our detector, we can approximate $k(t) = 1$.

Two further approximations can be done to simplify Equation 2. The first approximation consists in assuming the laser wavelength enough stable so that we can neglect the time dependence of λ . This approximation can be practically obtained using a commercial stabilized laser source. For example, the laser model 05-STP-903, produced by Melles-Griot© and used in our setup as laser source, has a (nominal) frequency of $f = 473.61254 THz$, a guaranteed frequency stability of $\Delta f = \pm 2.0 MHz$ and wavelength $\lambda = c/f = 632.8 nm$. The wavelength fluctuation is in this case $\Delta \lambda \approx 10^{-15} m$. Therefore, assuming a constant laser wavelength in our model, then we get a relative error of $\Delta \lambda / \lambda \approx 10^{-9}$, that is fully acceptable for our applications. Finally, for what concerns the intensity stability, the amplitude fluctuations of the laser source can be cancelled by monitoring the laser source power and normalizing the output of the interferometer.

The second approximation consists in assuming a constant and equal index of refraction in both arms. The index of refraction, one of the most significant parameters of the atmosphere for optical wave propagation, is very sensitive to small-scale temperature fluctuations. In fact, temperature fluctuations combined with turbulent mixing induce a random behavior in the field of atmospheric index of refraction. At the point \mathbf{R} in the space and time t , the index of refraction can be expressed by

$$n(\mathbf{R}, t) = n_0 + \Delta n(\mathbf{R}, t) \quad (5)$$

where $n_0 = \langle n(\mathbf{R}, t) \rangle \approx 1$ is the mean of the index of refraction and $\Delta n(\mathbf{R}, t)$ represents the random deviation, thus $\langle \Delta n(\mathbf{R}, t) \rangle = 0$. Normalizing the values of $n(\mathbf{R}, t)$ to n_0 , the fluctuations of the index of refraction can be related to corresponding temperature and pressure fluctuations. In particular, the index of refraction for the atmosphere can be written for optical and IR wavelengths as:⁶

$$n(R, t) = 1 + 77.6 \cdot 10^{-6} (1 + 7.52 \cdot 10^{-3} \lambda^{-2}) \frac{P(R, t)}{T(R, t)} \quad (6)$$

where λ is the optical wavelength in μm , P is the pressure in $mbar$, and T is the temperature in Kelvin. According

to this expression, the change in the refraction index can be expressed as:

$$\begin{aligned} \Delta n(R, t) = & +77.6 \cdot 10^{-6} (1 + 7.52 \cdot 10^{-3} \lambda^{-2}) \frac{1}{T(R, t)} \Delta P(R, t) \\ & - 1.17 \cdot 10^{-9} \lambda^{-3} \frac{P(R, t)}{T(R, t)} \Delta \lambda - \frac{1}{T^2(R, t)} \Delta T(R, t) \end{aligned} \quad (7)$$

As it is possible to see from this equation, the wavelength dependence is small for optical frequencies, that is positive since we use laser emitting in the optical and near infrared bands (from $0.4 \mu m$ up to $1.2 \mu m$). Moreover, since the pressure fluctuations are generally negligible, it is easy to see that the refractive index fluctuations associated with the visible and near infrared region of the spectrum are mainly due to random temperature fluctuations (humidity fluctuations only contribute in the far infrared region). Changes in the optical signal due to absorption or scattering by molecule or aerosols are not considered here.

An alternative approach is the following. If a more accurate measure is necessary, we can operate in this way. We define λ_n as the wavelength of the laser source in vacuum and λ_a as the laser wavelength in air. Therefore, the index of refraction is

$$n = \frac{\lambda_n}{\lambda_a} \quad (8)$$

and we can define the wavelength correction number (WCN) as the inverse of the index of refraction. This wavelength correction number can be derived by a direct measurement of the index of refraction with a refractometer or by using empirical data. If a refractometer is not available, it is preferable to measure the air pressure, temperature and relative humidity, and then to relate this data to the refractive index using the semi-empirical formulas obtained by Barrel and Sears⁷ and by Edlin⁸

$$WCN = \frac{1}{n} = \frac{10^6}{N + 10^6} \quad (9)$$

where

$$N = 0.3836391 P \cdot \left[\frac{1 + (0.817 - 0.0133 T) 10^6 \cdot P}{1 + 0.0036610 T} \right] - 3.033 \cdot 10^{-3} \cdot e^{-0.057627 T} \cdot H \quad (10)$$

and where the pressure P is measured in $mmHg$, the temperature T in degrees Celsius and the humidity in percentage %.

For example, assuming standard and homogeneous air composition, a one part-per-million error (ppm) will result from any one of the following condition:

- $1^\circ C$ change in air temperature;
- $2.5 mm$ of mercury change in the air pressure;
- 80% in relative humidity.

Equation 10 gives only an approximation of the refractive index, and thus it has some limitations related to the accuracy in measuring the atmospheric conditions. Generally it is possible to obtain an accuracy of $0.01 ppm$ using the Equation 10.

Therefore, as a conclusion, when the interferometer is in vacuum or positioned in a quiet and thermally stabilized environmental place, then the index of refraction can be considered constant at first level of approximation.

2.2 Transfer Function

To measure the transfer function of the interferometer for a seismic signal, we assume that the seismic wave $s(t)$ has its propagation vector k laying in the plane where the sensitive arm $l_2(t)$ of the interferometer is located, as shown in Figure 2. Therefore, the arrival of the seismic wave along the plane of the interferometer is sensed first by the end mirror M_2 and then, after a delay time t_0 , by the mechanical support, hosting the remaining

components of the interferometer (beam splitter BS , mirror M_1 , etc.). For simplicity, in our model we assume that the mechanical support is equivalent to a mass located at the beam splitter position.

Of course, due to its structure, the model is symmetric. In fact, the same seismic wave traveling in the opposite direction will be first sensed by the mechanical support, and then, after the same time delay t_0 , will be detected by the end mirror, M_2 .

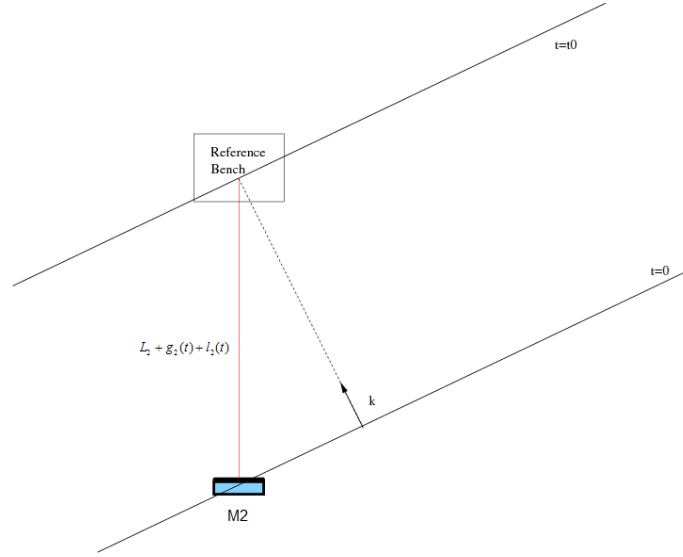


Figure 2. Scheme of interferometer response to a seismic wave

Let α be the angle between the wave vector k and the optical axes line l_2 , L_2 the position of the mirror M_2 , L_b the position of the mirror M_1 respect to the beam splitter, $g_b(t)$ the residual noise on the mirror M_1 , and v_s the wave group velocity of signal $s(t)$, then t_0 can be written as:

$$t_0 = \frac{[L_2 + g_2(t) + s(t)] \cos \alpha}{v_s} \quad (11)$$

where $g_2(t)$ quantifies the residual noise on the mirror M_2 , filtered by the mechanical transfer function of the mounting.

For $t > t_0$ the wave front moves both the mirror and the optical lengths become:

$$\begin{aligned} l_1(t) &= L_b + g_b(t) \\ l_2(t) &= L_2 + g_2(t) + [(s(t) - a_s s(t - t_0)) \cos(\alpha)] \end{aligned} \quad (12)$$

where a_s is the attenuation factor expressing the ratio of the seismic wave amplitude at the second mirror with respect to the first one ($0 \leq a_s \leq 1$). In this way the phase changes as

$$\phi(t) = \frac{4\pi n}{\lambda} [L_2 - L_b + g_2(t) - g_b(t) + (s(t) - a_s s(t - t_0)) \cos(\alpha)] \quad (13)$$

Let $\Delta L(t) = [L_2 - L_b] + g_2(t) - g_b(t)$ be the length change in absence of signal, then the relationship in the Laplace domain between the seismic signal $s(t)$ and the phase is

$$\phi(s) = \frac{4\pi n}{\lambda} [\Delta L(s) + S(s) (1 - a_s e^{-t_0 s}) \cos(\alpha)] \quad (14)$$

The transfer function of the system that links the input seismic signal $s(t)$ with the Michelson phase change $\phi(s)$ can be written as

$$H(s) = \frac{\phi(s)}{S(s)} = \frac{4\pi n}{\lambda} (1 - a_s e^{-t_0 s}) \cos(\alpha) \quad (15)$$

while the transfer function for the noise can be written as

$$H_n(s) = \frac{\phi(s)}{\Delta L(s)} = \frac{4\pi n}{\lambda} \quad (16)$$

that shows that the interferometer is fully sensitive to all local micronoise (mechanical, refraction index changes, etc.).

Let us now analyze the behavior of the interferometer in the limit of short arm-length with respect to the seismic waves wavelengths. In this case the delay time t_0 becomes small and it is possible to expand $e^{-t_0 s}$ in Taylor series as

$$\begin{aligned} H(s) &= \frac{4\pi n}{\lambda} \cos(\alpha) \left(1 - a_s \sum_{k=0}^{\infty} \frac{s^k}{k!} \frac{d^k e^{-t_0 s}}{ds^k} \Big|_{t_0=0} \right) \\ &= \frac{4\pi n}{\lambda} \cos(\alpha) \left((1 - a_s) + a_s \sum_{k=1}^{\infty} \frac{s^k}{k!} \frac{d^k e^{-t_0 s}}{ds^k} \Big|_{t_0=0} \right) \end{aligned} \quad (17)$$

Having assumed a short arm-length interferometer, then we can neglect the terms of the Taylor series with $k > 1$ of Taylor series and assume an attenuation factor $a_s = 1$. In this way the relation between the input seismic signal $s(t)$ and the output Michelson phase change $\phi(t)$ can be written in the Laplace domain as:

$$\phi(s) = \frac{4\pi n}{\lambda} \cos(\alpha) t_0 s S(s) \quad (18)$$

and then in the time domain as

$$\phi(t) = \frac{4\pi n}{\lambda} \cos(\alpha) t_0 \left(U(t - t_0) \frac{ds(t)}{dt} \right) \quad (19)$$

This means that, according to the above hypothesis, the phase, $\phi(t)$, is proportional, at least at the first order, to the input signal derivative, and, therefore, to the velocity of the seismic waves. In the following we evaluate the harmonic response of the interferometer to seismic signals whose wavelengths are much larger than the interferometer arm-lengths. Using the explicit form of t_0 , the harmonic response is:

$$H(j\omega) = \frac{4\pi n}{\lambda v_s(j\omega)} j\omega \cos^2(\alpha) \quad (20)$$

where $v_s(j\omega)$ is the velocity of seismic wave at angular frequency ω . To show the angular dependence of the instrument sensitivity, we plotted the sensitivity diagram according to equation 20 (see Figure 3).

It can be easily seen that this diagram has the classical shape of a dipole, in which the maximum sensitivity is for $\alpha = 0$ and $\alpha = \pi$ and the minimum sensitivity is for $\alpha = \pi/2$ and $\alpha = 3\pi/2$. According to this diagram it is easy also to conclude that it is possible to build an omni-directional instrument for seismic waves measurement, by simply using two Michelson interferometers oriented perpendicularly each other.

The only point still to discuss is how to extract the function $\phi(t)$ by the measurement of the interferometer intensity through the output photodiode. For this task it is necessary the inversion of Equation 1 to obtain

$$\phi(t) = \cos^{-1} \left[2 \frac{I(t) - I_{min}}{I_{max} - I_{min}} - 1 \right] \quad (21)$$

Particular care is needed in the application of this formula. In fact, if during the selected time interval the output intensity of the interferometer reaches its maximum or minimum value, then the Equation 21 is not longer valid due to the periodicity of the cosine function. Physically, it means that the interferometer is passing from the working fringe to the next one. The method used to solve this problem is presented in T.R. Judge and P.J. Bryanston-Cross (1994).⁹ Therefore, to evaluate the free mirror acceleration with respect to the reference arm, it is sufficient to numerically derive Equation 19:

$$a(t) = \frac{d^2 s(t)}{dt^2} = \frac{\lambda}{4\pi n t_0 \cos(\alpha)} \dot{\phi}(t) \quad (22)$$

Equation 19 has been approximated using only the first term of the Taylor series expansion of $H(s)$ as shown in Equation 17, thus introducing then error due to the Taylor series truncation. This error can be quantified using the formula of the remainder Taylor series:

$$R_n(t_0) = \int_0^{t_0} f^{(n+1)}(t) \frac{(t - t_0)^n}{n!} dt$$

Therefore, if we keep only the first term of the Taylor series, then we make an error equal to

$$R_2 = \left\| \frac{3\pi^2 f^2 L^4}{v_s^4} \right\| \tag{23}$$

In Figure 4 the Taylor series truncation error is shown for our prototype ($L = 0.2 m$) as function of the seismic wave frequency.

2.3 Data Acquisition

As it is well known from the Nyquist theorem, the sampling frequency F_c must be at least twice the maximum frequency of the output signal of the Michelson Interferometer, $I(t)$. Thus the sampling frequency F_c should be

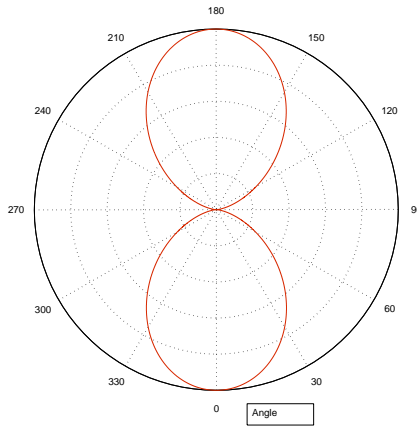


Figure 3. Normalized sensitivity diagram for a Michelson interferometer with free mirror in the $0 rad$ direction.

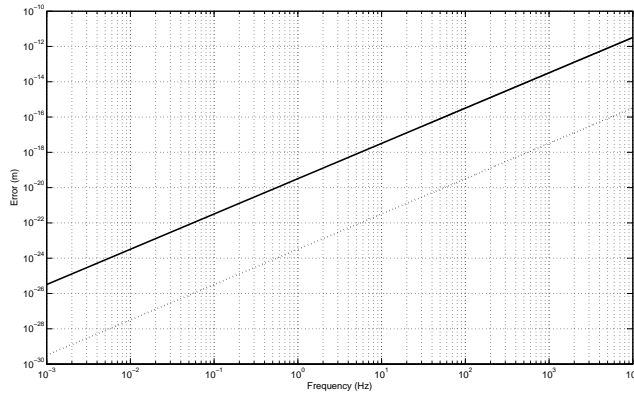


Figure 4. Phase error due to Taylor series truncation.

higher than $\dot{\phi}(t)/\pi$, where $\dot{\phi}(t)$ is the velocity of the phase. Being the phase given by the equation:

$$\phi(t) = \frac{4\pi n t_0}{\lambda} \frac{ds(t)}{dt} \quad (24)$$

and the propagation time is $t_0 = L/v_s$, then the instantaneous frequency of $I(t)$ is:

$$f(t) = \frac{\dot{\phi}}{2\pi} = \frac{2nL}{\lambda v_s} \frac{d^2s(t)}{dt^2} \quad (25)$$

It is also possible to choose the sampling frequency using as requirement the maximum acceleration a_p measured by the instrument. In fact, since the sampling frequency is related to the phase derivative by the relation:

$$F_c > 2f_{max} = \frac{\dot{\phi}}{\pi} \quad (26)$$

hence it is possible to determine the minimum sampling frequency as a function of the instrument parameters:

$$F_c > \frac{4nL}{\lambda v_m} a_p \quad (27)$$

where the peak acceleration a_p is a calibration parameter and v_m is the expected minimum wave velocity.

3. EXPERIMENTAL APPARATUS

The experimental apparatus used as prototype for a laser interferometry based seismic sensor consists mainly of a Michelson interferometer in air, an accelerometer for comparison, a digital acquisition system to get data from these instruments and to store them in an electronic archive. A triaxial episensor (model FBA ES-T, from Kinematics©) is located close to the interferometer to monitor the acceleration in that point. The episensor is made of three independent accelerometers oriented in the different directions of the space. In this way the probe can measure the accelerations along the three spatial axis: x , y and z . The user selectable full scale of all the accelerometers was chosen at $\pm g/4$, where g is the standard gravitational acceleration while the voltage output level is fixed at $20 V$. Using an instrument amplifier implemented by us, the acceleration signal is amplified by a factor 100. In this configuration the episensor sensitivity is $\pm 800 V/g$. The frequency band nominally spans from DC to $200 Hz$, while the nominal dynamic range is $155 dB$, according to the instrument specifications.

3.1 Optical setup

A scheme of the implemented interferometer test system is shown in Figure 5.

The light beam coming from the laser is sent to a first beam-splitter B_{s1} . The reflected beam is sent to the photodiode Ph_1 used to monitor the light source power, while the transmitted one is split again by the second beam-splitter B_{s2} and, after the reflection of the two resulting beams on the end mirrors M_1 and $M-2$, is finally recombined on the interferometer output photodiode Ph_2 . The arm-lengths of the interferometer are about $20 cm$. An optical isolator, located between the laser and the first beam-splitter, prevents the backscattering of light toward the laser source. A phase modulator, managed by a lock-in amplifier, is placed along the fixed arm. All the optical elements of the interferometer are fixed to an optical bench with $30 cm$ high and $60 cm$ wide.

3.2 Electronic setup and Data Acquisition

The signals coming from the photodiodes, from the lockin amplifier and from the episensor are collected by an acquisition system. This is composed by an analog pre-processing board followed by the analog to digital converter (ADC) board. The analog pre-processing consists in amplifying the signals to fit their amplitude to the ADC converters dynamic range. All the chain is shown in Figure 6.

The signals are filtered with suitable anti-aliasing filters. In our experiment we use a 16-bit ADCs, so that we have a dynamic range of $96 dB$. The implemented antialiasing filter guarantees that, for sampling frequencies above the frequency of about $470 Hz$, the aliasing error is lower than the ADC noise. The filter is an eight order

Chebyshev low pass filter with a band pass ripple of 0.5 dB and a cut-off frequency of 200 Hz . Each filter used in the acquisition system was characterized to ensure that its behavior matches with the one used in the calculated response. The digital converter consists of a VME board equipped with a 16 bit ADC with 32 channels. The sampling frequency, F_s , is fixed at 5000 Hz for the tests, in order to guarantee very good performances of the antialiasing filters. According to equation 27, in this configuration the instrument is able to measure a maximum acceleration of

$$a_p < \frac{\lambda v_m F_s}{4nL} \approx 3.15 \frac{m}{s^2} \tag{28}$$

for $v_m \approx 800\text{ m/s}$, as calculated in the next paragraph.

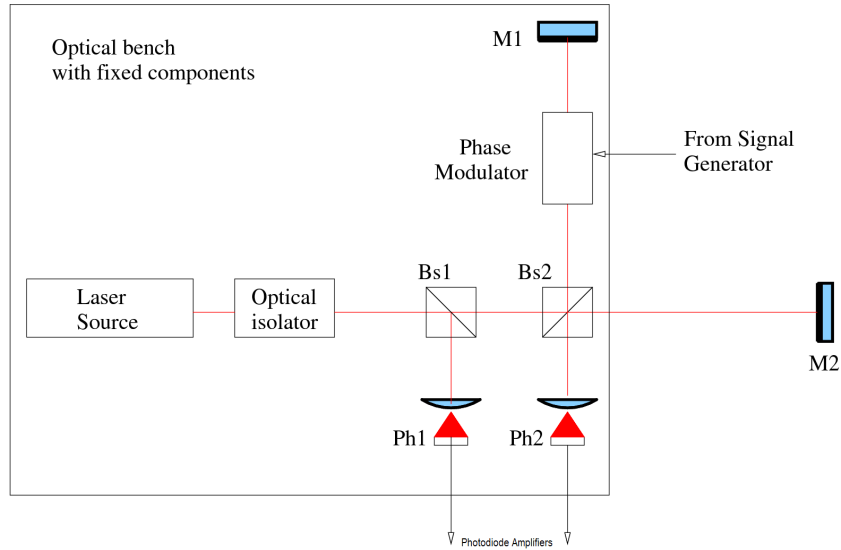


Figure 5. Optical setup of our prototype (not in scale).

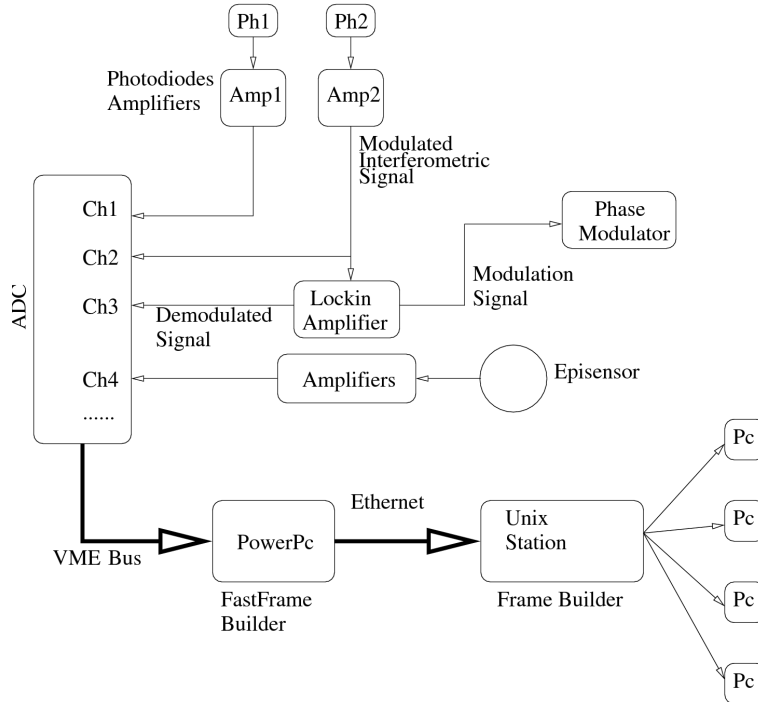


Figure 6. Data Acquisition system.

Actually the phase shift induced by the filtering is not significant for the following analysis, because all signals are affected by the same shift. The sampling frequency is generated by an internal clock of the ADC board and the general timing system is simply the CPU clock. This arrangement is very useful during the test phase, but in order to setup a complete measurement system, a GPS timing board is necessary to provide a precise timing to perform coincidence with other seismic stations.

The ADC board is managed by a PowerPC CPU based computer board on VME bus, running LynxOS operating system. The CPU collects the data acquired by the ADC and pack them in frames, each frame 1 second long. These frames are then sent to a workstation through a Fast Ethernet network for the analysis. The frames are then packed together in groups of defined length and then analyzed in real-time, since the analysis process does not require high computing power. The processed data are packed again and sent to another workstation, equipped with a very large hard disk space, for the final storage.

Preliminary tests of data acquisition are being also performed with a prototype of hybrid acquisition and control system with an on-board communication link designed developed by our group.¹⁰ This solution has the advantage of allowing the collection of data into a control station and the actuation/tuning with a maximum sampling frequency ranging of $f_c > 40 kHz$ with a standard protocol over an Enhanced Parallel Port (EPP). The goal is to use this system in the next future, replacing the one reported in Figure 6.

4. EXPERIMENTAL RESULTS

In this section we present and discuss the experimental results of the implemented prototype. To reduce the influence of the acoustic noise, the interferometer has been protected with a cover. Of course, the environmental effects can be controlled and reduced only by monitoring the pressure and temperature of air.

With reference to Figure 5, it is easy to see that the fluctuations of the interference signal from photodiode Ph_2 can be reduced using the signal from photodiode Ph_1 . In fact, if there is a change $\Delta I(t)$ in the laser power $I(t)$, then photodiode Ph_1 measures the quantity

$$Ph_1(t) = k(I(t) + \Delta I(t)) \quad (29)$$

where k is the fraction of the laser beam separated by the beam splitter (in theory k is 0.5). The photodiode Ph_2 measures the quantity

$$Ph_2(t) = \frac{(1-k)(I(t) + \Delta I(t))}{2} [1 + C \cos(\phi(t))] \quad (30)$$

where C is the visibility of the fringes. If we evaluate the ratio

$$\frac{Ph_2(t)}{Ph_1(t)} = \frac{(1-k)}{2k} [1 + C \cos(\phi(t))] \quad (31)$$

it is easy to see that it is possible to cancel, at least at the first order, the laser power fluctuations $\Delta I(t)$.

The first step of the procedure is the quadrature correction to normalize the interferometer signal and the lockin signal in the range $[-1 : 1]$. After the phase correction, the phase unwrapping algorithm is applied to recover the interferometer phase without ambiguity.⁹ Then the ground acceleration can be evaluated using the Equation:

$$a_k(t) = a_x(t) \cos(\alpha) = \frac{d^2 s(t)}{dt^2} = \frac{\lambda}{4\pi n t_o} \dot{\phi}(t) \quad (32)$$

where a_x is the acceleration along the sensitive arm of the interferometer and a_k is the seismic wave. The numerical derivative of the phase is evaluated using the central differences algorithms approximating the derivative as

$$\frac{d\phi(t)}{dt} \approx \frac{\phi(n+1) - \phi(n-1)}{2\Delta t} \quad (33)$$

In Figure 7 the power spectral density of the acceleration measured by the episenor and by the interferometer is shown. It is easy to verify the good agreement between the two instruments in the band $0.5 \div 100 Hz$. The signal at frequency $\approx 17 Hz$ must be yet understood.

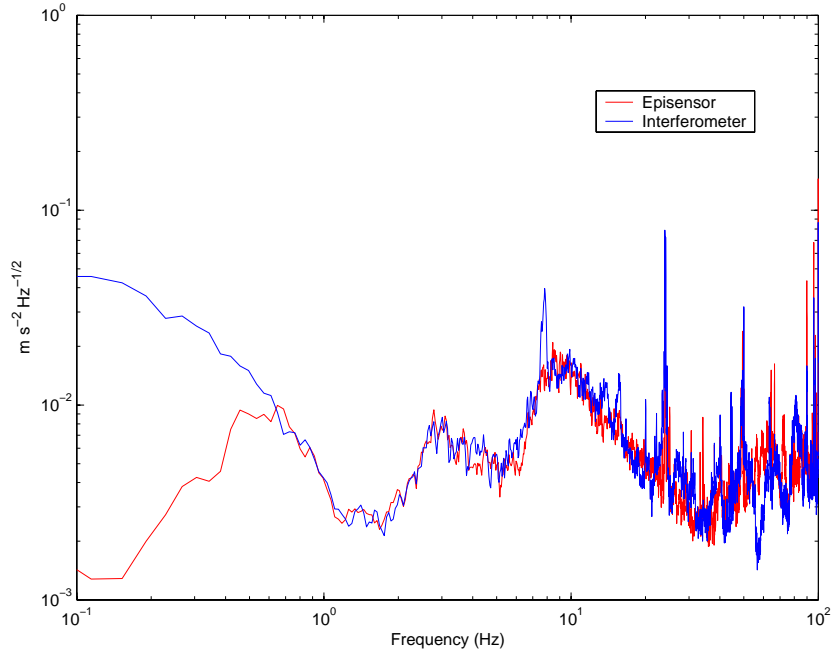


Figure 7. Psd of the acceleration measured by the episensor and by the protected interferometer.

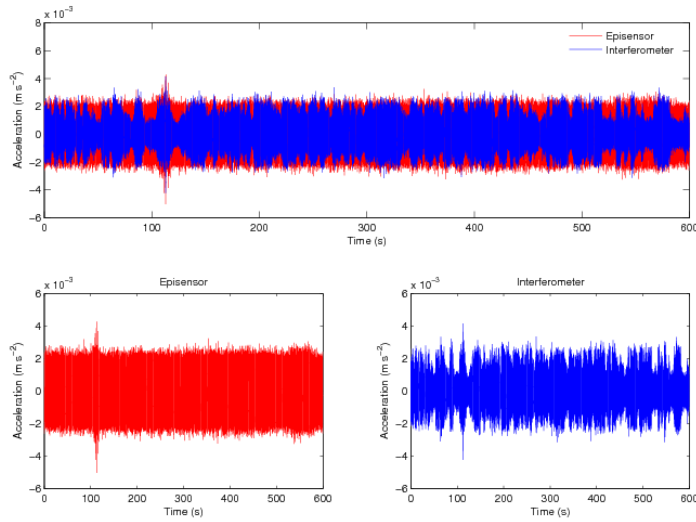


Figure 8. Time evolution of acceleration measured by the episensor and by the interferometer.

The empirical value t_0 is evaluated comparing the power spectral density of the acceleration measured by the episensor and by the interferometer. Considering the interferometer arm-length ($L = 0.2 \text{ m}$), then the velocity on the ground of the acoustic waves in our laboratory results about 800 m/s . The decreasing of the sensitivity in the low frequency band is probably due to the laser frequency noise and to the fluctuations of the index of the refraction. We have to consider also that in the case of a low frequency wave, the wave velocity can be so high that the sampling frequency may be not enough high to measure the fringe frequency, reducing the sensitivity at low frequency.

In Figure 8 the time evolution of the acceleration measured by the episensor and by the interferometer is shown. As it can be seen, the sensitivity of the interferometer is enough to show a particular structure in the

data: in fact the acceleration measured by the interferometer seems composed by separable different signals. A more accurate analysis is, therefore, necessary to understand the sources of these signals. Note that these signals are not clearly present in the episenor output, probably due to the high noise level at high frequency.

5. CONCLUSIONS

We demonstrated that a very simple array of two Michelson Interferometers can be used as an effective seismic sensor, with an output proportional to the velocity of seismic waves. Main limitations of this sensor are environmental parameters like temperature and pressure, whereas the effects of laser intensity changes can be cancelled at least at the first order. Experimental tests of this technique, using a single Michelson Interferometer, confirm the theoretical results, allowing interferometric measurements of the ground waves speed that is in good agreement with the measurements provided by a state-of-the-art commercial accelerometer for seismic applications. The results obtained are very encouraging, so that we are upgrading the system in order to measure the local acceleration of the mirrors and beam splitter of the velocimeter using ad hoc designed monolithic accelerometers for low frequency direct measurement of the seismic noise.¹¹

REFERENCES

1. F. Acernese, R. De Rosa, F. Garufi, R. Romano, F. Barone, *A Michelson Interferometer for seismic wave measurement: theoretical analysis and system performances*, in Proc. of SPIE *Remote Sensing for Environmental Monitoring, GIS Applications, and Geology VI*, edited by M. Ehlers and U. Michel, Stockholm, Sweden, September 11-16, SPIE Vol.6366, 63660I1-11 (2006).
2. J. Berger and J. Levine, *The spectrum of earth strain from 10^{-8} to 10^2 Hz*, *J. Geophys. Res.*, vol.79, no.1210, 1974.
3. M. Born and E. Wolf, *Principles of Optics*, Pergamon Press, Oxford, 1964.
4. F. Acernese, F. Barone, R. De Rosa, L. Milano, *Interferometric sensor for seismic noise measurement: theoretical model and experimental performances*, in Proc. of SPIE *Europe International Symposium Remote Sensing*, 13-16 September 13-16, Maspalomas, Canary Islands, Spain (2004).
5. F. Acernese, R. De Rosa, F. Garufi, R. Romano, F. Barone *Laser Interferometric Sensor for seismic waves measurement*, SPIE Sensors and Smart Structures technologies for Civil, Mechanical, and Aerospace Systems 2007, edited by Masayoshi Tomizuka, Chung-Bang Yun, Victor Giurgiutiu, Proc. SPIE Vol.6529, 65292F-1-12 (2007).
6. L. C. Andrews and R. L. Phillips, *Laser Beam Propagation through Random Media*, Vol. PM53 of SPIE Press Monograph Series (SPIE, Bellingham, Wash., 1998).
7. H. Barrel and J.E. Sears, *Phil Trans. Roy. Society*, A258, pp. 1-64, 1936.
8. B. Edelin, *The Refractive Index of the air*, Metrologia, Vol.2, No.2, 71, 1966.
9. T. R. Judge and P. J. Bryanston-Cross, *A review of phase unwrapping techniques in fringe analysis*, Optics and Lasers in Engineering, Vol.21, pp199-239, 1994.
10. F. Garufi, F. Acernese, A. Boiano, R. De Rosa, R. Romano, F. Barone *Hybrid control and acquisition system for distributed sensors for environmental monitoring*, SPIE Smart Structure 2007, in Sensor Systems and Networks: Phenomena, Technology, and Application for NDE and Health Monitoring 2007, edited by Kara J. Peters, Proc. SPIE Vol.6530, 65301M1-6 (2007).
11. F. Acernese, R. De Rosa, G. Giordano, R. Romano, F. Barone *Mechanical Monolithic Sensor for low frequency seismic noise measurement*, SPIE Sensors and Smart Structures technologies for Civil, Mechanical, and Aerospace Systems 2007, edited by Masayoshi Tomizuka, Chung-Bang Yun, Victor Giurgiutiu, Proc. SPIE Vol.6529, 65292B1-12 (2007).